Article

Numerical Investigation of the Electro-Thermo Convection in an Inclined Cavity Filled with a Dielectric Fluid

Dalila Akrour [1], Mohamed Issam Elkhazen [2], Walid Hassen [2], Karim Kriaa [3,4,*], Chemseddine Maatki [5], Bilel Hadrich [3] and Lioua Kolsi [6,*]

[1] Theoretical and Applied Fluid Mechanics Laboratory, Faculty of Physics USTHB, Bab-Ezzouar, Algiers 16111, Algeria; dalila_akrour@yahoo.com

[2] Laboratory of Metrology and Energy Systems, University of Monastir, Monastir 5000, Tunisia; mohamedissam.khazen@ksarhelal.r-iset.tn (M.I.E.); hassen.walid@gmail.com (W.H.)

[3] Department of Chemical Engineering, College of Engineering, Imam Mohammad Ibn Saud Islamic University (IMSIU), Riyadh 11432, Saudi Arabia; bmhadrich@imamu.edu.sa

[4] Department of Chemical Engineering, National School of Engineers of Gabes, University of Gabes, Gabes 6029, Tunisia

[5] Department of Mechanical Engineering, College of Engineering, Imam Mohammad Ibn Saud Islamic University (IMSIU), Riyadh 11432, Saudi Arabia; casmaatki@imamu.edu.sa

[6] Department of Mechanical Engineering, College of Engineering, University of Ha'il, Ha'il City 81451, Saudi Arabia

[*] Correspondence: kskriaa@imamu.edu.sa (K.K.); lioua_enim@yahoo.fr (L.K.)

Abstract: The present work is a numerical analysis of electro-thermo convection, occurring in a square differentially heated cavity filled with a dielectric fluid. The cavity experiences the combined effects of viscous, electrical, and thermal forces. The equations modelling the physical problem are solved via the finite volume approach. The study focuses on the effect of cavity tilt on the fluid flow structure and thermal performance inside the enclosure under the action of an electric field. A parametric study was performed, where the tilt angle is getting varied between 0° and 90°, as well as the Rayleigh number (5000 ≤ Ra ≤ 250,000) and the electric field (0 ≤ T ≤ 800). Furthermore, the electric charge injection level C, the mobility M and the Prandtl Pr numbers were all adjusted to a value of 10. The obtained results demonstrate that the hydrodynamic and thermal fields are significantly impacted by the cavity inclination. In addition, regardless of the thermal Rayleigh's number, high electric field values could govern fluid movement through electric forces. Electro-convection typically demonstrates an oscillating flow due to the tilting of the cavity which gives rise to a bicellular regime occupying the entire cavity. A correlation has been established to estimate heat transfer by considering various system parameters such as cavity inclination, electrical Rayleigh number, and thermal Rayleigh number.

Keywords: cavity inclination; electro-thermo-convection; buoyancy forces; electric field; numerical simulation; finite volume method

1. Introduction

Electric field combined to heat transfer has garnered growing consideration in the past few years due to its wide scope of benefits in many engineering fields, such as the formation of crystals in a liquid, nuclear reactors cooling, electronic equipment thermal dissipation, as well as microelectronic devices, solar technology, fuel cells [1], etc. During the last decades, several leading journals covered various issues of electrohydrodynamic improvement of heat transfer [2–4] within square, cylindrical, and elliptical cavities. An intensive study of EHD convection was given by Hassen et al. [2].

However, cavity inclination can also have a significant influence on heat transfer encountered in both industrial and natural fields. Existing literature includes numerous works relating to the subject, without the electric field and/or, in the presence of a magnetic field.

Numerical studies carried out by Mourabit et al. [5] examined the effect of 'T' shape cavity inclination equipped with heating blocks. The flow behavior and heat transfer rate in the case of mixed convection have been studied. The authors found that tilt promotes cooling of the left block and disadvantages cooling of the right block.

Cheong et al. [6], have examined free convection in a tilted rectangular cavity with a sine-wave temperature applied on the left wall. Streamlines, isotherms, and Nusselt numbers are illustrated and studied. It was noticed that heat exchange decreases with increasing cavity tilt for all aspect ratios of the simulated geometries. The authors established a correlation to quantify the mean Nusselt number by considering the thermal Rayleigh number, cavity tilts angle, and form factors as variables.

Yekani et al. [7] have also numerically analyzed the free convection of a nanofluid in a porous enclosure with differentially heated vertical surfaces, the numerical simulations have been carried out for various porous Grashof numbers and for different inclinations of the enclosure (from $0°$ to $60°$). The numerical findings reveal the existence of a boundary layer adjacent to the walls of the enclosure, and its thickness diminishes as the porosity decreases or the porous Grashof number increases.

Ouyahia et al. [8] investigate numerically the impact of tilt on magnetohydrodynamic, laminar-free convection within a rectangular cavity containing an Al_2O_3-water nanofluid. This cavity was subjected to a horizontal, constant, and uniform magnetic field. The vertical walls were differentially heated, and the inclination was varied between $0°$ and $60°$. It was found that the variation of the tilt angle leads to changes in the structure of the flow. Indeed, the best thermal performances were obtained for an angle of inclination of $30°$, unlike $60°$ which has the lowest Nusselt number values.

Benyoucef et al. [9] have investigated the 3D convection of a tilted rectangular cavity filled with silicone oil and compared it with experimental results. A complex behavior has been detected, the increase in the angle beyond $0°$ destabilizes the convective pattern to benefit from an unstable situation for specific Rayleigh number values. The authors demonstrated that the mean Nusselt number achieves more rapid convergence to the stationary state when the angles fall within the range of $25°$ to $60°$.

Hakan et al. [10] used the heatline visualization technique to visualize the heat transport in a non-isothermally heated square inclined (from $0°$ to $90°$) cavity filled with water-CuO nanofluid. The authors showed that for low Ra around 10^3, increasing the angle of inclination leads to an improvement in the Nusselt number. For Ra = 10^4 and 10^5, the average Nusselt number decreases as the angle of inclination are varied from $30°$ to $60°$ and increases again between $60°$ and $90°$.

Vivek et al. [11] conducted a numerical study to analyze the effects of the interaction between surface radiation and natural convection in air-filled tilted enclosures. The study covered a wide range of tilt angles (α). The authors have shown that the presence of surface radiation results in an enhancement of the overall convective circulation rate for specific tilt angles. The Convective Nusselt number reaches its maximum value at an angle of $\alpha = +15°$ and remains unaffected by the presence or absence of radiation. The significance of the interaction effects between radiation and convection is much higher in shallow enclosures compared to square enclosures. In a shallow cavity with an aspect ratio of 5, a positive inclination of $45°$ reduces convection by 50%, while negative inclinations increase convection by more than 100%.

Very recently, Mandal et al. [12] studied the effect of a magnetic field on free convection in an inclined porous cavity with corrugated walls. The cavity was filled with $Cu-Al_2O_3$/water hybrid nanofluid and partially heated from the top and bottom walls. It has been found that heat transfer and air movement increase with the inclination of the cavity. The direction of the magnetic field and the volume fraction of the added nanoparticles are also parameters that control heat transfer.

Several quite recent experimental studies have also focused on natural convection in inclined cavities. Leporini et al. [13] experimentally studied the behavior of natural convection in an inclined square cavity with hot side walls and a cold bottom wall. Four different cavity inclination angles, from 0 to 90°, and five different hot wall temperatures ($10^4 \leq$ Ra $\leq 10^5$) were tested for a total of 20 different conditions. The techniques adopted for the experimental tests are particle image velocimetry (PIV) to determine velocity fields and a set of thermocouples to measure wall temperature. It has been determined that both the average and maximum velocities exhibit an increase as the Rayleigh number and tilting angle increase. The velocity field exhibits two vortices, with a symmetry axis crossing, the center of the enclosure when the tilt angle is 90°; as this angle increases, the symmetry tends to disappear, resulting in the presence of only one vortex for 90°.

Abdulmunem et al. [14] published an experimental study to investigate the effects of different tilt angles on the melting of a PCM material (paraffin wax) inside a rectangular enclosure. Four different angles ranging from 0 to 90° were tested by subjecting a single wall to a constant temperature of 373 Kelvin. Heating was carried out using a 1000 W sun simulator to achieve a uniform heat distribution across the surface of the plate. A total of 10 K-type thermocouples were strategically positioned within the paraffin wax to facilitate accurate measurements of temperature. The authors show that the overall melting time increases by more than 75% when the cavity tilt angle is reduced from 90 to 0°. It was also noted that decreasing the angle of inclination reduces the effect of convective heat transfer during MCP melting until a purely conductive heat transfer state is reached at 0°.

This literature review unequivocally illustrates the impact of cavity tilt which is important to control heat transfer as well as flow patterning. However, as far as we are aware, no previous study has examined this effect in the presence of an electric field. Therefore, the main goal of this paper is to assess the hydrodynamic and thermal performance of a dielectric fluid enclosed within an inclined cavity under the action of an electric field. The influence of the tilt angle, the electric and thermal Rayleigh numbers, on heat transfer and flow topography was illustrated and discussed.

2. Physical Model and Governing Equations

The geometry in question is a layer of insulating (dielectric) liquid located in a square cavity of dimension L^2 (Figure 1). The bottom and top surfaces are thermally insulated, while the side surfaces are differentially heated and held at a constant and homogenous temperature (with θ_H denoting the hot side and θ_C the cold one). To achieve an enhanced heat exchange, a potential difference is created between the horizontal surfaces. The bottom wall serves as the emitting electrode and is maintained at the highest potential (V_i). The top wall is maintained at the lowest potential (V_0) which is considered as the receiving electrode.

The fluid is considered Newtonian, incompressible and isotropic. Also, based on theoretical [15–20] and numerical [21–29] studies, the injected charges are supposed to be autonomous and homogeneous, implying that these charges density at the emitting electrode is consistently maintained to an unchanging value q_0.

The fundamental equations governing this problem, using the Boussinesq approximation are as follows [27–29].

Mass equation

$$\nabla . \vec{U} = 0. \tag{1}$$

Momentum equation

$$\rho \frac{d\vec{U}}{dt\prime} = -\nabla p + \rho \vec{g} \beta (\theta - \theta_0) + \mu \nabla^2 \vec{U} + q\vec{E}. \tag{2}$$
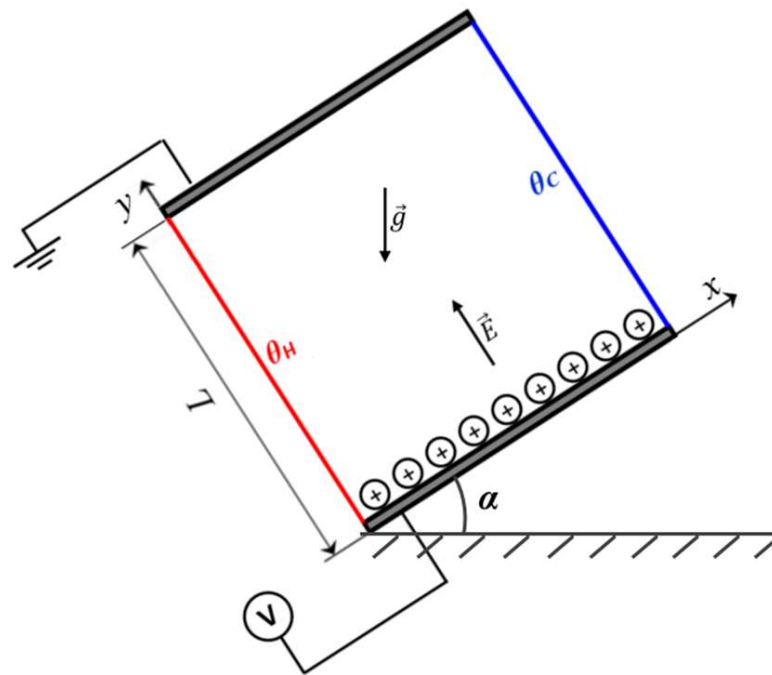
Figure 1. Physical model.

Thermal energy equation

$$\rho C_P \frac{d\theta}{dt} = \lambda \nabla^2 \theta. \tag{3}$$

Maxwell's conservation equations

$$\frac{\partial q}{\partial t} + \nabla \cdot \vec{j} = 0 \text{ where } \vec{j} = q\left(\vec{U} + K\vec{E}\right), \tag{4}$$

$$\nabla \cdot (\varepsilon \vec{E}) = q, \tag{5}$$

$$\vec{E} = -\nabla V. \tag{6}$$

As a numerical approach, the "Vorticity-Current function" [30] (ψ-ω) formalism was adopted, using the following variable changes:

$$U_x = \left(\frac{\partial \psi}{\partial y}\right), \tag{7}$$

$$U_y = -\left(\frac{\partial \psi}{\partial x}\right), \tag{8}$$

$$\omega = \left(\frac{\partial U_y}{\partial x} - \frac{\partial U_x}{\partial y}\right). \tag{9}$$

To describe problems universally, it is especially useful to work with dimensionless equations. For this purpose, the following transformations are conducted,

$$x^* = \frac{x}{L} \qquad y^* = \frac{y}{L} \qquad U_x^* = U_x \frac{L}{\nu} \qquad U_y^* = U_y \frac{L}{\nu} \qquad \psi^* = \frac{\psi}{\nu} \qquad \omega^* = \omega \frac{L^2}{\nu}$$

$$t^* = t \frac{\nu}{L^2} \qquad \theta^* = \frac{(\theta - \theta_C)}{(\theta_H - \theta_C)} \qquad q^* = \frac{q}{q_0} \qquad E^* = E \frac{L}{(V_0 - V_1)} \qquad V^* = \frac{(V - V_1)}{(V_0 - V_1)}$$

$$\omega = -\left(\frac{\partial^2 \Psi}{\partial x^2} + \frac{\partial^2 \Psi}{\partial y^2} \right), \tag{10}$$

$$\frac{\partial \omega}{\partial t} + U_x \frac{\partial \omega}{\partial x} + U_y \frac{\partial \omega}{\partial y} = \frac{\partial^2 \omega}{\partial x^2} + \frac{\partial^2 \omega}{\partial y^2} + \frac{Ra}{Pr} \left(\cos \alpha \frac{\partial \theta}{\partial x} - \sin \alpha \frac{\partial \theta}{\partial y} \right) + \frac{CT^2}{M^2} \left(\frac{\partial(qE_y)}{\partial x} - \frac{\partial(qE_x)}{\partial y} \right), \tag{11}$$

$$\frac{\partial \theta}{\partial t} + U_x \frac{\partial \theta}{\partial x} + U_y \frac{\partial \theta}{\partial y} = \frac{1}{Pr} \left(\frac{\partial^2 \theta}{\partial x^2} + \frac{\partial^2 \theta}{\partial y^2} \right), \tag{12}$$

$$\frac{\partial q}{\partial t} + \frac{\partial}{\partial x} \left(q \left(U_x + \frac{T}{M^2} E_x \right) \right) + \frac{\partial}{\partial y} \left(q \left(U_y + \frac{T}{M^2} E_y \right) \right) = 0, \tag{13}$$

$$\frac{\partial^2 V}{\partial x^2} + \frac{\partial^2 V}{\partial y^2} = -C \cdot q, \tag{14}$$

$$E_x = -\frac{\partial V}{\partial x}, \tag{15}$$

$$E_y = -\frac{\partial V}{\partial y}. \tag{16}$$

In the above-mentioned equations, five dimensionless numbers are defined as follows:

$$Pr = \frac{\nu}{a} \qquad Ra = \frac{g \cdot \beta \cdot \Delta\theta \cdot L^3}{\nu \cdot a} \qquad C = \frac{q_0 \cdot L^2}{\varepsilon \cdot \Delta V} \qquad T = \frac{\varepsilon \cdot \Delta V}{\rho \cdot \nu \cdot K} \qquad M = \frac{1}{K} \left(\frac{\varepsilon}{\rho} \right)^{\frac{1}{2}}.$$

The thermal characteristic of the system is represented by the Rayleigh number Ra and the Prandtl number Pr. Ra denotes the quotient of thermal force and the viscous resistance force, whereas Pr is the momentum to thermal diffusivities ratio. The remaining three numbers are related to the electrical side. The electric Rayleigh number T describes the electric Coulomb force to viscous force. The injection level is denoted by C, and the dimensionless ionic mobility is represented by M.

The boundary and initial conditions are expressed in the following manner:

For t = 0

$$\omega = \Psi = \frac{\partial \Psi}{\partial y} = \frac{\partial \Psi}{\partial x} = \theta = V = q = 0 \quad \text{in all the studied areas.}$$

For t > 0

$$\Psi = \frac{\partial \Psi}{\partial y} = 0; \ \theta = 1; \ \frac{\partial q}{\partial x} = \frac{\partial V}{\partial x} = 0 \quad \text{for } x = 0 \ \text{(hot wall)},$$

$$\Psi = \frac{\partial \Psi}{\partial y} = 0; \ \theta = 0; \ \frac{\partial q}{\partial x} = \frac{\partial V}{\partial x} = 0 \quad \text{for } x = 1 \ \text{(cold wall)},$$

$$\Psi = \frac{\partial \Psi}{\partial y} = 0; \ \frac{\partial \theta}{\partial y} = 0; \ q = V = 1 \quad \text{for } y = 0 \ \text{(adiabatic emitter electrode)},$$

$$\Psi = \frac{\partial \Psi}{\partial y} = 0; \ \frac{\partial \theta}{\partial y} = 0; \ V = 0; \ \frac{\partial q}{\partial y} = 0 \quad \text{for } x = 1 \ \text{(adiabatic collector electrode)},$$

To quantify the heat transfer level, we employ the following equations to calculate both the local and average Nusselt numbers:

$$\mathrm{Nu_{loc}} = -\left.\frac{\partial \theta}{\partial x}\right|_{x=0}, \tag{17}$$

$$\mathrm{Nu_{Av}} = \int_0^1 -\left.\frac{\partial \theta}{\partial x}\right|_{x=0} \mathrm{dy}. \tag{18}$$

3. Numerical Method

The partial differential equations (PDEs) (7) to (12) and the related boundary conditions are resolved by performing numerical integration over a control volume. The power law scheme, described in [31], has been employed to handle the convective terms. The time derivative terms are discretized using a semi-implicit Euler first-order scheme, as described in reference [30]. The semi-implicit first order Euler time scheme was chosen to discretize the temporal derivatives terms. This choice was made in order to improve the precision and reliability of the solution. The scheme relies on a hybrid approach comprising explicit and implicit components, where the explicit part is used to approximate the nonlinear terms and the implicit part is used to approximate the linear terms. This combination ensures that the numerical solution is stable and accurate, and also allows for a fast convergence of the numerical solution.

After discretization, a system of algebraic equations is generated for variables such as temperature, stream function, vorticity, electric potential, and charge density. To solve this system, the Successive Over Relaxation technique (SOR) is employed, utilizing the Gauss–Seidel iterative solver [31]. To guarantee the reliability of the results, grid independency checks were conducted to determine the optimal mesh size for the simulation. After a series of tests, it was found that a 101×101 control volume mesh was sufficient to obtain the required precision. The dimensionless time step must be chosen carefully to guarantee the stability of the calculations, for this reason a small enough time step of 10^{-4} is found adequate to serving this purpose while stills being computationally efficient [32]. The numerical solution can be considered as converged and the SOR algorithm can be stopped when the following convergence criterion is being verified.

$$\frac{\max\left|\psi^{k+1} - \psi^k\right|}{\max\left|\psi^k\right|} + \max\left|q^{k+1} - q^k\right| + \max\left|\theta^{k+1} - \theta^k\right| \leq 10^5, \tag{19}$$

where the exponent k denotes the kth step of the successive overrelaxation method.

For further details about the calculation methodology, please consult the paper by Hassen et al. [33].

4. Results and Discussion

In this section, the combined effect of the cavity tilt (from 0° to 90°) coupled to an electric field in the presence of a temperature gradient is investigated. This refers to the rotation of the cavity in a clockwise direction, which enables the study of various geometries ranging from the position where the thermal gradients are perpendicular to gravity ($\alpha = 0$) to the Rayleigh–Bénard situation ($\alpha = 90$) where gravity counteracts thermal gradients. Liquid gas oil is selected as the working medium. The thermophysical properties of this fluid, detailed in [34], enable the calculation of both the Prandtl number and the ionic mobility, with values set to Pr = M = 10. The charge injection level is classified into three regimes [35]: strong (C > 5), medium (0.2 < C < 5), and weak (0 < C < 0.2). Among these regimes, previous studies have mainly opted for strong injection with C = 10, which seems to be the most widely used choice. The thermal and electrical Rayleigh numbers as well as the inclination angle were the subject of the parametric study. As shown in Table 1,

the parametric study begins by investigating the impact of inclination ($0 \leq \alpha \leq 90$) while keeping Ra and T constant, and then explores the effect of inclination under various applied electric fields ($0 \leq T \leq 800$) and different imposed thermal gradients ($5000 \leq Ra \leq 250,000$).

Table 1. Parametric study details.

Study Setup	Ra	T	α
Effect of Tilt angle	50,000	600	
Effect of Tilt angle for various electric field	10,000	0–800	0–90
Effect of Tilt angle for various thermal gradient	5000–250,000	200	

Figure 2 presents the steady-state charge density distribution, streamlines, and isothermal lines plots for Ra = 50,000 and T = 600. In the case of 0° tilt, it is clearly seen that the collaboration between the thermal and the electric field on the right side of the cavity generates a sudden acceleration of the cell rotational speed. The flow structure is characterized by a circular vortex with a center shifted to the hot wall. The distortions of the isothermal lines are so pronounced in the center of the cavity that a thermal gradient inversion takes place. On the other hand, on the upper right and lower left corners, a strong intensification of this gradient is observed. As for the electric charge distribution, we can also identify the inversion of the gradient from the center to more accentuated near to the isothermal walls.

Tilting the cavity up to 30° results in a slight 10% increase in vortex velocity, but no significant alteration in the flow topography is observed. Above an inclination of 45°, a bifurcation from a single-cell flow to a two-cell flow is noted.

This bifurcation can be explained by the fact that the cavity inclination causes a reduction in the intensity of buoyancy forces (going from $\rho \cdot g \cdot \beta \cdot \Delta\theta$ to $\rho \cdot g \cos \alpha \cdot \beta \cdot \Delta\theta$), while the electrical forces remain unaffected. However, the left portion of the cavity is the location of collaboration between the electrical and thermal forces, generating a large and intense cell and a strong penetration of electrical charge. For isothermal lines, this also leads to a division of the cavity into two compartments. A hot and dominating left compartment and a cold one on the right side.

The same configuration persisted until 60°; however, when an angle of 90° was reached, two horizontally oriented and symmetric counter-rotating cells were observed. These cells are located at the top and bottom regions of the cavity.

Figure 3 presents both the temporal evolution of the mean and local Nusselt number on the hot wall. Two different behaviors for heat transfer can be distinguished. For an angle $\alpha \in [0, 40°]$, an increase in the angle of tilt results in a 5% improvement in heat transfer. From 45°, called the critical angle which separates the one-cell regime from the two-cell regime, an oscillatory regime appears, leading to a significant decrease (around 33%) in the Nusselt number. By further increasing the tilt angle, the amplitude, and frequency of the oscillations increase, leading to a subsequent increase in heat transfer.

Finally, it is essential to point out that the bottom part of the hot wall experiences the most intense heat exchange, particularly for 'y' values ranging from 0.25 to 0.3. Conversely, the top section of the heated wall exhibits inefficient heat transfer, regardless of the cavity's angle.
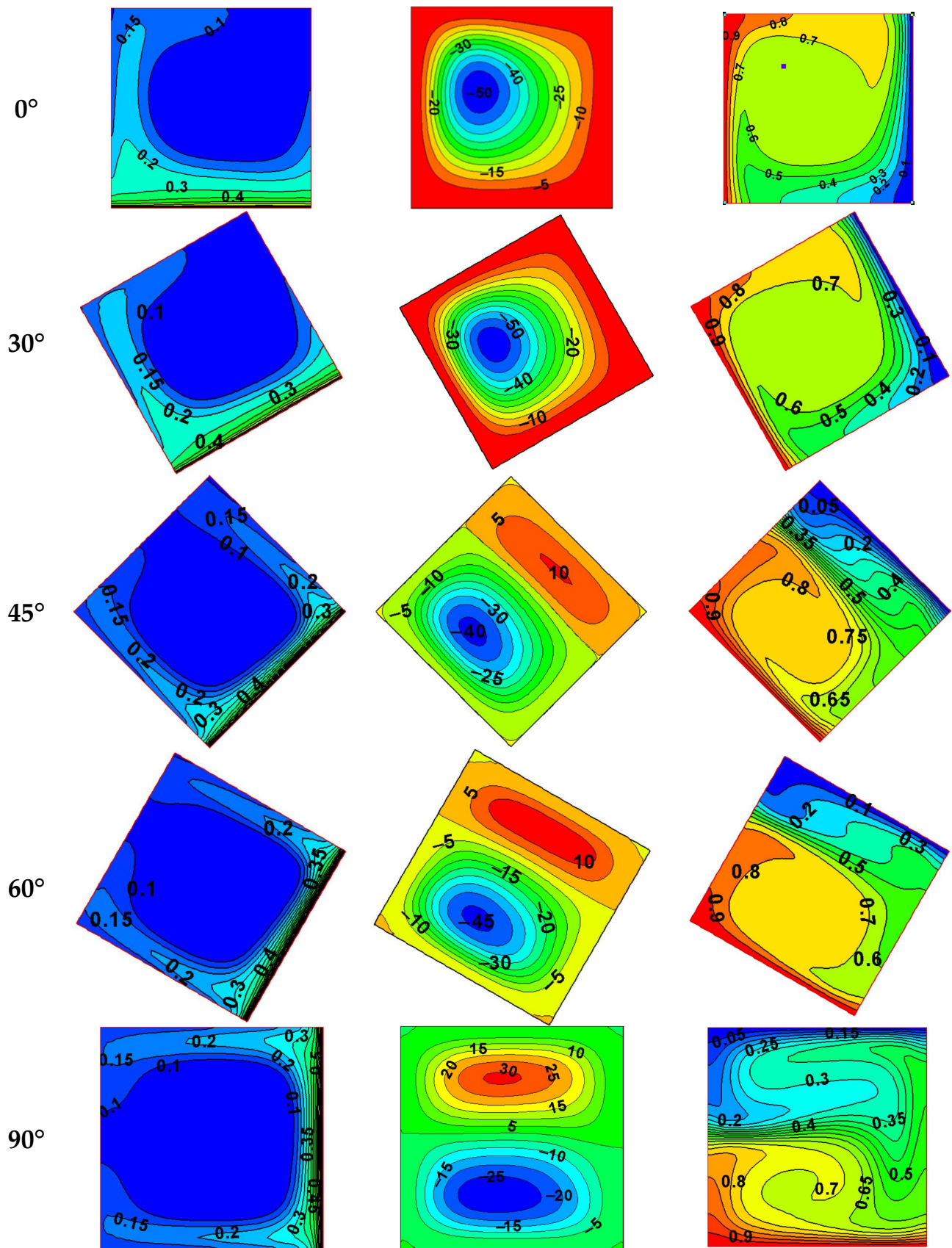
Figure 2. Charge density distributions (**left**), streamlines (**middle**), and isothermal lines (**right**) for Ra = 50,000, T = 600, Pr = 10, C = 10, for different tilt angles.

(a)

(b)
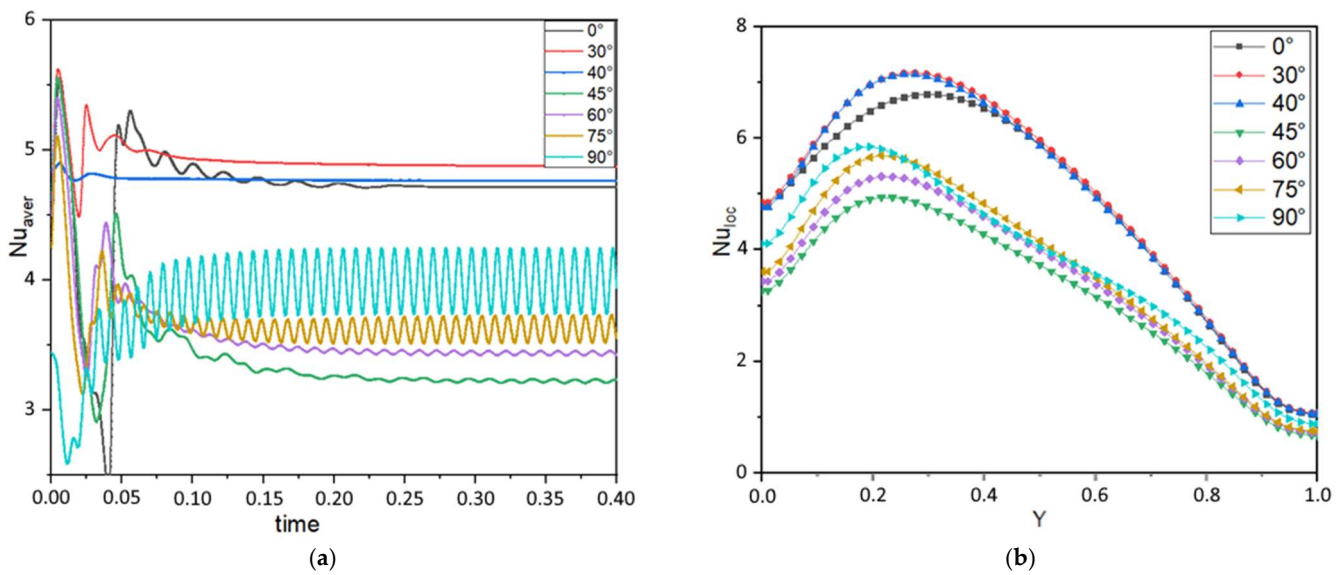
Figure 3. (**a**) Time profile of the average Nusselt number; (**b**) local Nusselt number on the hot plate for Ra = 50,000 and T = 600 and for various inclinations.

Charge density distributions for various tilt angles and electrical Rayleigh numbers are illustrated in Figure 4. At an extremely low electrical Rayleigh number (T = 10), thermal forces dominate, and buoyancy forces entirely dictate the movement of electric charges. Indeed, electric charges exhibit an upward orientation in the vicinity of the hot wall, while they manifest a downward direction close to the cold wall. This creates a kind of ring inside the cavity. The inclination of the cavity seems to have no impact on the charge density distribution. Conversely, for a large electric Rayleigh number (T = 600), electrical forces take control. Both electric plumes along the vertical walls take place regardless of the cavity's tilt. Finally, for a moderate electrical Rayleigh number. A single plume originates along the hot wall, where the thermal and electrical forces cooperate. However, on the cold wall side, the downward thermal forces seem to be more dominant for $\alpha = 0$ and $45°$, preventing the development of a second plume. In this case (moderate T value), the cavity inclination affects the charge density distribution topography. As the angle α reaches $90°$ a shift occurs from a single-plume pattern to a bifurcated-plume arrangement situated at both the upper and lower regions of the cavity. For $\alpha = 0°$, the charge distribution aligns closely with the findings reported by Hassen et al. [36] and Traore et al. [37].

T = 10   T = 200   T = 600

0°
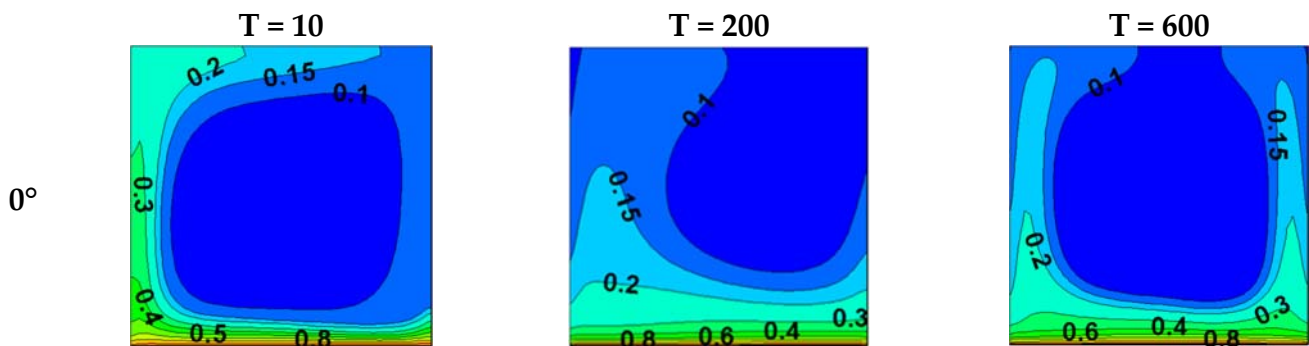
Figure 4. *Cont.*
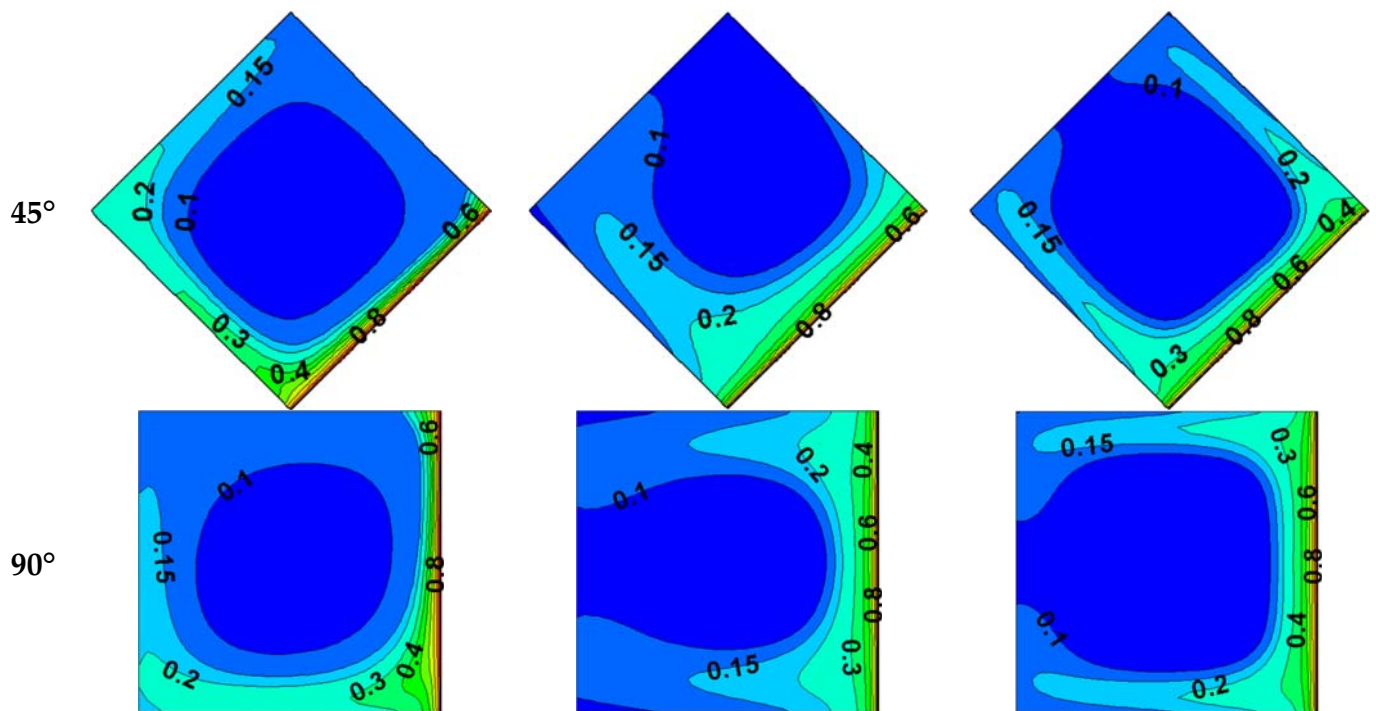
Figure 4. Distributions of charge density for different tilt angles and for different values of the electric Rayleigh number, Ra = 10,000, Pr = 10, C = 10, and M = 10.

The local Nusselt number variation over the hot wall according to the tilt angle is plotted in Figure 5. At T = 10, heat exchange occurs mainly in the lower part of the heated wall. For y < 0.4, the heat transfer is more significant as the inclination angle decreases. In fact, for y = 0.1, a difference of 45% in Nu number is observed between $\alpha = 0°$ and $\alpha = 90°$, indicating the impact of the inclination angle on heat transfer. However, in the upper half of the hot wall, the heat transfer is slightly affected by the cavity inclination. By increasing the electric field strength, the impact of the tilt angle becomes less important, even in the lower part of the hot plate. For T = 600, regardless of the tilt angle, almost all the curves overlap. This was expected due to the intensification of the electric field, which reaches a level where the flow regime is electrically dominated, and it becomes the only parameter controlling the heat transfer process.

The mean Nusselt number according to the tilt cavity for various T values is shown in Figure 6. Two distinct behaviors can be recorded for T ≤ 200, as depicted in Figure 6a. The profile of the mean Nusselt number follows a parabolic shape with a maximum around an angle of 45°. It is interesting to report that the outcomes for T = 10 and T = 0 are identical. This similarity arises because, for a low Rayleigh number, T < Tc below the critical Rayleigh number (commonly referred to as the linear stability criterion [37]) the electric field has an insignificant impact on natural convection. Increasing T leads to a thermal transfer enhancement of approximately 13% between T = 0 and 200. For high values of T (greater than 400), a reduction in Nu can be observed between 200 and 400 due to bifurcations from a single-cell flow to a two-cell flow. Further, increasing T results in the intensification of the average Nusselt number, reaching an improvement of 61% between T = 0 and T = 800. It should also be noted that for high electrical Rayleigh values, the profile of the average Nusselt number exhibits horizontal lines, indicating that the electrical forces are so dominant that the cavity tilt has no influence on the heat exchange process, and the only controlling parameter is the electrical force.

T = 10

T = 200

T = 600
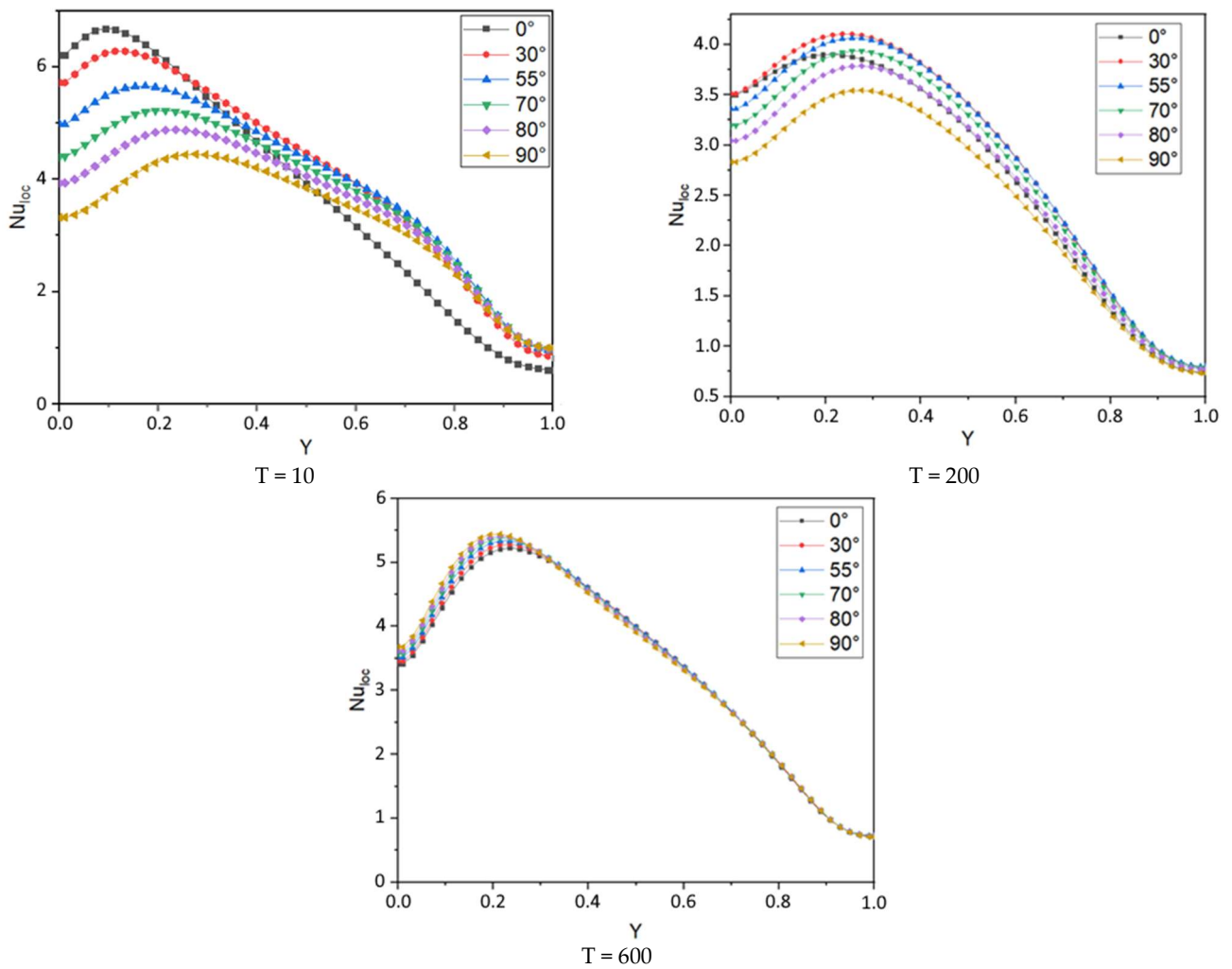
Figure 5. Local Nusselt number on the hot wall for Ra = 50,000, Pr = 10, C = 10, M = 10, and various cavity inclination angles.

(**a**)

Figure 6. *Cont*.

(**b**)
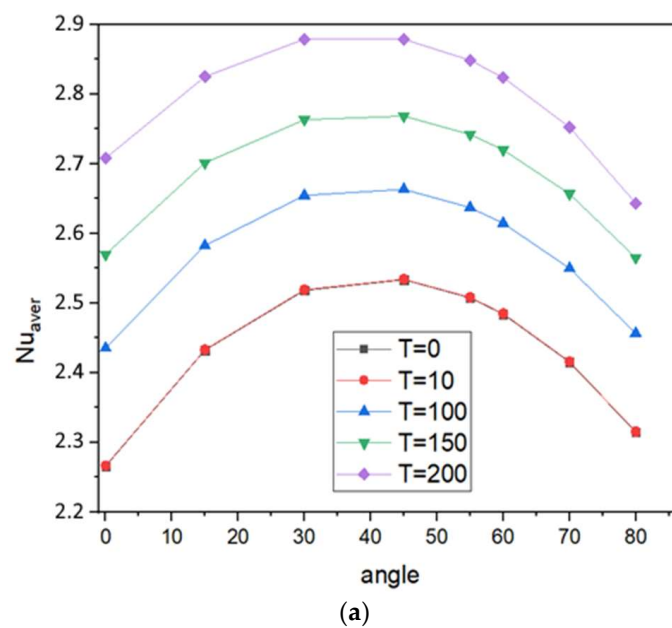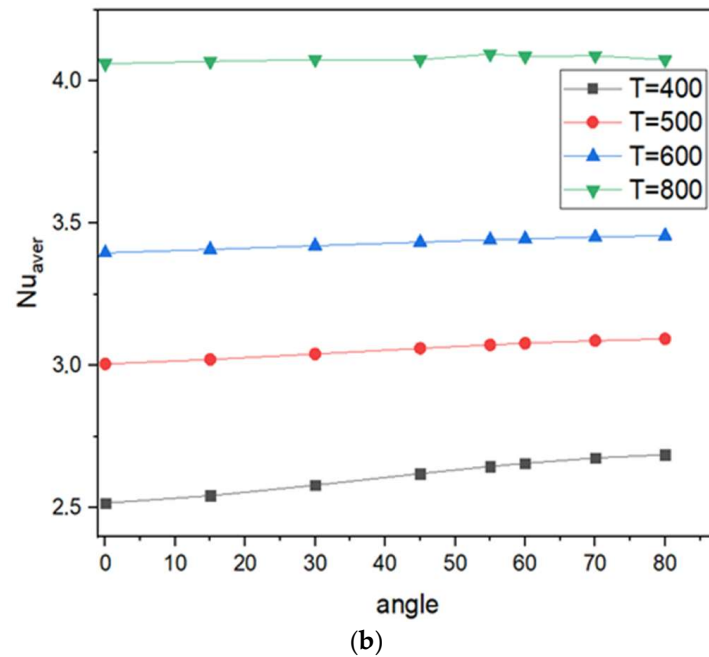
Figure 6. Average Nusselt number according to tilt cavity angle for Ra = 10,000, Pr = 10, C = 10, and M = 10 and various T values (**a**) $0 \leq T \leq 200$ (**b**) $400 \leq T \leq 800$.

Figure 7 plots the evolution of the local Nusselt number with respect to the cavity inclination angle for different Rayleigh numbers. It can be shown that convective heat exchange is more significant when the thermal Rayleigh number is higher. An intensification of up to 180% is achieved at an angle of 15° just by increasing Ra = 5000 to 250,000. However, we observe that the Nusselt number is only affected by inclination when the thermal Rayleigh number is relatively high (Ra > 10^5). Moreover, for high Ra values, the optimal heat exchanges are reached at 15–30° cavity inclination, while a reduction of 34% occurs at an angle of 90°.
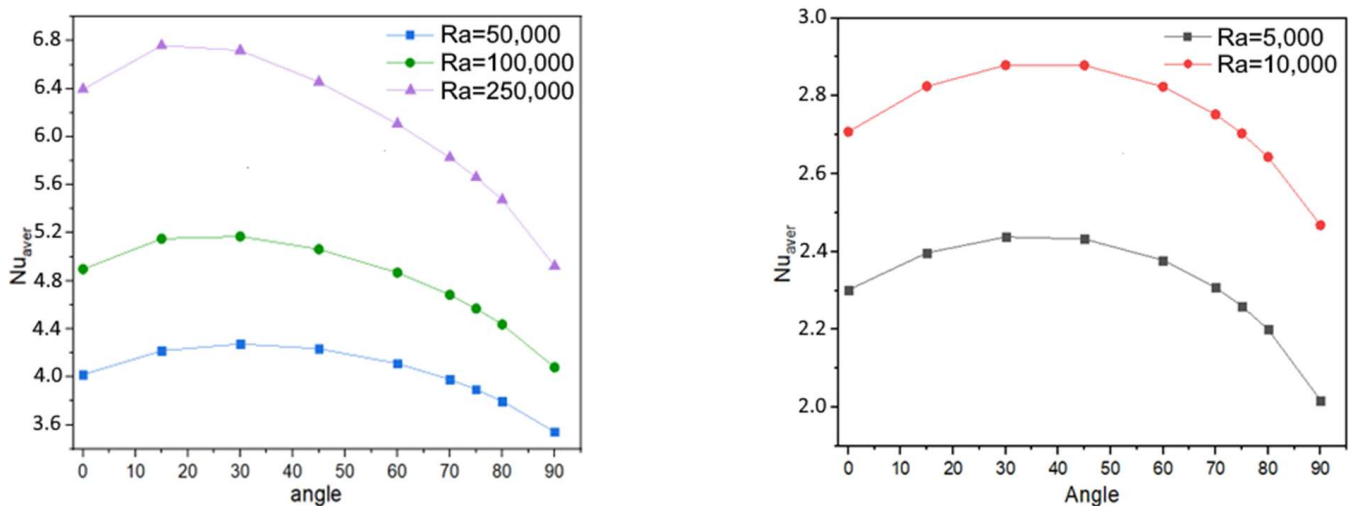
Figure 7. Average Nusselt number according to tilt cavity angle for T = 200, Pr = 10, C = 10, M = 10, and various Ra values.

After conducting several numerical simulations, a multi-parameter linear regression analysis was performed to establish an empirical correlation. Although several correlations have been presented in the literature for estimating the Nusselt number in the case of classical free convection in inclined cavities, such as those suggested by Wright et al. [38], ElSherbiny et al. [39], and Khezzar et al. [40]. As far as our current knowledge extends, no correlation has yet been suggested for the case of electro-thermo convection, taking into account the inclination angle, heat transfer, and electric field.

The correlation proposed in Equation (17) offers an approximate estimation of the Nusselt number, which is applicable for a wide range of thermal Rayleigh numbers, spanning from 5000 to 250,000, electrical Rayleigh numbers ranging from 10 to 600, and tilt angles varying between 0° and 80°.

$$NU = 0.221 \ Ra^{0.242} \ T^{0.061} \ \exp(-0.011 \ \tan(\alpha)). \tag{20}$$

This correlation exhibits a coefficient of determination $R^2 = 0.95$, a standard error $\sigma = 0.06$, and a *p*-value for the different parameters ranging from 0 to 0.007. All these statistical parameters, such as the *p*-value, standard deviation, and coefficient of determination, indicating the effectiveness and reliability of the proposed correlation.

To further confirm the validity of the correlation, comparison tests were carried out in Figure 8. These tests compare the mean values of the Nusselt number (Nu) simulated and given by Equation (20) for several influential parameters (Ra, T, and α). The excellent agreement between simulated and correlated mean Nusselt numbers highlights the good reliability of the developed correlation. Indeed, the maximum error does not exceed 4%, confirming the accuracy of Equation (20).
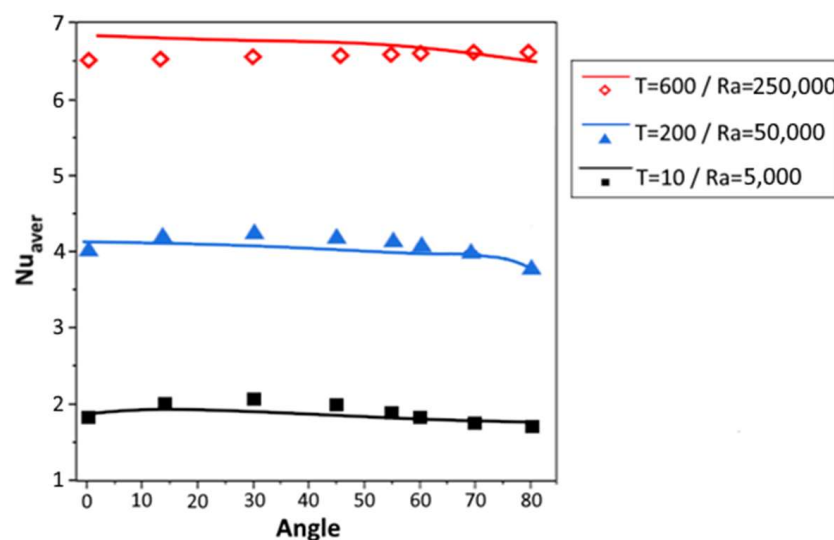
Figure 8. Average Nusselt number according to tilt cavity angle for various Ra and T numbers lines: Correlation values; Symbols: Numerical results.

5. Conclusions

In this work, numerical simulations of elelctro-thermo convection in an inclined differential-heated square cavity have been carried out. The cavity is filled with dielectric fluid and subjected to an electric field. A parametric study was conducted to investigate the effects of enclosure inclination, imposed thermal gradient, and applied electric field. The key conclusions of this study can be outlined in the following:

- The flow's behavior can be significantly impacted by the inclination of the cavity. By increasing this angle, a shift from a unicellular to a bicellular regime was detected.

- At high electric and thermal fields, when the angle $\alpha \in [0, 40°]$, increasing the tilt angle results in a 5% improvement in heat transfer. Above this angular range, an oscillation regime could be developed.
- Local Nusselt numbers show that heat exchange occurs mainly in the lower section of the heated wall. A reduction in the convective heat transfer of up to 45% can be recorded when the angle varies from 0 to 90 degrees.
- Increasing the electrical Rayleigh number (up to 800) and the thermal Rayleigh number (to 250,000) results in a respective improvement of 61% and 181% in heat transfer.
- For high electrical Rayleigh values, the dominant electrical forces negate the impact of cavity tilt on heat transfer.
- A multiparametric correlation was suggested to estimate the mean Nusselt number, based on the tilt angle, and both thermal and electrical Rayleigh numbers.

Author Contributions: Conceptualization, D.A., M.I.E., W.H., K.K., C.M. and L.K.; Methodology, M.I.E., W.H., K.K. and B.H.; Validation, D.A. and L.K.; Formal analysis, D.A., M.I.E., W.H. and C.M.; Investigation, D.A., M.I.E., B.H. and L.K.; Writing—original draft, D.A., M.I.E., W.H., K.K., C.M., B.H. and L.K.; Writing—review & editing, D.A., M.I.E., W.H., K.K., C.M., B.H. and L.K. All authors have read and agreed to the published version of the manuscript.

Data Availability Statement: Not applicable.

Conflicts of Interest: The authors declare no conflict of interest.

Nomenclature

a	Thermal diffusivity ($m^2 \cdot s^{-1}$)
C	Dimensionless number of the injection strength
$\vec{E}$	Electric field ($V \cdot cm^{-1}$)
$\vec{g}$	Acceleration of gravity ($m \cdot s^{-2}$)
K	Ionic mobility ($m^2 \cdot V^{-1} \cdot s^{-1}$)
L	Enclosure width (m)
M	Dimensionless number which characterizes EHD properties of the liquid
Pr	Prandlt number
q	Electric charge density ($C \cdot m^{-3}$)
Ra	Thermal Rayleigh number
T	Dimensionless electric Rayleigh number
t	Time (s)
$\vec{U}$	Velocity ($m \cdot s^{-1}$)
V	Electric potential (V)
x,y	Cartesian coordinate (m)
Greek symbols	
α	cavity inclination (°)
β	Coefficient of thermal expansion of fluid (K^{-1})
ε	Permittivity of the fluid ($F \cdot m^{-1}$)
θ	Dimensionless temperature (K)
μ	Dynamic viscosity ($Pa \cdot s$)
ν	Kinematic viscosity ($m^2 \cdot s^{-1}$)
ϱ	Density ($kg.m^{-3}$)
ψ	Stream function ($m^2 \cdot s^{-1}$)
ω	Vorticity (s^{-1})
Subscript	
H	Hot
C	Cold

References

1. Shang, Z.; Hossain, M.M.; Wycisk, R.; Pintauro, P.N. Poly (phenylene sulfonic acid)-expanded polytetrafluoroethylene composite membrane for low relative humidity operation in hydrogen fuel cells. *J. Power Sources* **2022**, *535*, 231375. [CrossRef]
2. Hassen, W.; Elkhazen, M.I.; Traore, P.; Borjini, M.N. Charge injection in horizontal eccentric annuli filled with a dielectric liquid. *Eur. J. Mech. B/Fluids* **2018**, *72*, 691–700. [CrossRef]
3. Zhou, C.T.; Yao, Z.Z.; Chen, D.L.; Luo, K.; Wu, J.; Yi, H.L. Numerical prediction of transient electrohydrodynamic instabilities under an alternating current electric field and unipolar injection. *Heliyon* **2023**, *9*, e12812. [CrossRef] [PubMed]
4. Selvakumar, R.D.; Wu, J.; Huang, J.; Traoré, P. Electro-thermo-convection in a differentially heated square cavity under arbitrary unipolar injection of ions. *Int. J. Heat Fluid Flow* **2021**, *89*, 108787. [CrossRef]
5. Mourabit, M.; Rouijaa, H.; Semma, E.A.; Alami, M.E.; Najam, M. Etude numérique de l'effet d'inclinaison d'une cavité en forme de 'T'sur la symétrie de la solution et le transfert de chaleur. *J. Renew. Energy* **2014**, *17*, 519–527.
6. Cheong, H.T.; Siri, Z.; Sivasankaran, S. Effect of aspect ratio on natural convection in an inclined rectangular enclosure with sinusoidal boundary condition. *Int. Commun. Heat Mass Transf.* **2013**, *45*, 75–85. [CrossRef]
7. Motlagh, S.Y.; Taghizadeh, S.; Soltanipour, H. Natural convection heat transfer in an inclined square enclosure filled with a porous medium saturated by nanofluid using Buongiorno's mathematical model. *Adv. Powder Technol.* **2016**, *27*, 2526–2540. [CrossRef]
8. Ouyahia, S.; Benkahla, Y.K.; Benzema, M.; Berabou, W. Effet du champ magnétique sur la convection naturelle dans une cavité inclinée remplie d'un nanofluide. In Proceedings of the Congrès de la Société Française de Thermique, Larochelle, France, 31 May–3 June 2015.
9. Benyoucef, D.; Zeroual, M.; Benmoussa, H. Natural convection in tilted rectangular cavities due to bidirectional temperature gradient. *Int. J. Heat Technol.* **2017**, *35*, 883–892. [CrossRef]
10. Oztop, H.F.; Mobedi, M.; Abu-Nada, E.; Pop, I. A heatline analysis of natural convection in a square inclined enclosure filled with a CuO nanofluid under non-uniform wall heating condition. *Int. J. Heat Mass Transf.* **2012**, *55*, 5076–5086. [CrossRef]
11. Vivek, V.; Sharma, A.K.; Balaji, C. Interaction effects between laminar natural convection and surface radiation in tilted square and shallow enclosures. *Int. J. Therm. Sci.* **2012**, *60*, 70–84. [CrossRef]
12. Mandal, D.K.; Mondal, M.K.; Biswas, N.; Manna, N.K.; Chamkha, A.J. Partial magnetic field and segmental heating effects on hybrid nanofluidic convection in a tilted porous wavy cavity. *J. Magn. Magn. Mater.* **2023**, *583*, 171035. [CrossRef]
13. Leporini, M.; Corvaro, F.; Marchetti, B.; Polonara, F.; Benucci, M. Experimental and numerical investigation of natural convection in tilted square cavity filled with air. *Exp. Therm. Fluid Sci.* **2018**, *99*, 572–583. [CrossRef]
14. Abdulmunem, A.R.; Samin, P.M.; Rahman, H.A.; Hussien, H.A.; Mazali, I.I.; Ghazali, H. Experimental and numerical investigations on the effects of different tilt angles on the phase change material melting process in a rectangular container. *J. Energy Storage.* **2020**, *32*, 101914. [CrossRef]
15. Castellanos, A.; Atten, P.; Pérez, A.T. Finite-amplitude electroconvection in liquids in the case of weak unipolar injection. *Physicochem. Hydrodyn.* **1987**, *9*, 443–452.
16. Felici, N. Phénomenes hydro et aérodynamiques dans la conduction des diélectriques fluides. *Rev. Gen. Electr.* **1969**, *78*, 717–734.
17. Atten, P.; Lacroix, J.C. Non-linear hydrodynamic stability of liquids subjected to unipolar injection. *J. Mec.* **1979**, *18*, 469–510.
18. Watson, P.K.; Schneider, J.M.; Till, H.R. Electrohydrodynamic stability of space-charge-limited currents in dielectric liquids. II. Experimental study. *Phys. Fluids* **1970**, *13*, 1955–1961. [CrossRef]
19. Lacroix, J.C.; Atten, P.; Hopfinger, E.J. Electro-convection in a dielectric liquid layer subjected to unipolar injection. *J. Fluid Mech.* **1975**, *69*, 539–563. [CrossRef]
20. Atten, P.; Lacroix, J.C. Electrohydrodynamic stability of liquids subjected to unipolar injection: Non linear phenomena. *J. Electrost.* **1978**, *5*, 439–452. [CrossRef]
21. Castellanos, A.; Pérez, A.T.; Chicon, R. Chaotic electroconvection in a layer of dielectric liquid subjected to unipolar injection: Maximal Lyapunov exponents. *Int. J. Bifurc. Chaos Appl.* **2002**, *12*, 2523–2534. [CrossRef]
22. Suh, Y.K. Modeling and simulation of ion transport in dielectric liquids-Fundamentals and review. *IEEE Trans. Dielectr. Electr.* **2012**, *19*, 831–848.
23. Adamiak, K. Numerical models in simulating wire-plate electrostatic precipitators: A review. *J. Electrost.* **2013**, *71*, 673–680. [CrossRef]
24. Pérez, A.T.; Castellanos, A. Role of charge diffusion in finite-amplitude electroconvection. *Phys. Rev. A* **1989**, *40*, 5844. [CrossRef]
25. Traoré, P.; Wu, J. On the limitation of imposed velocity field strategy for Coulomb-driven electroconvection flow simulations. *J. Fluid Mech.* **2013**, *727*, R3. [CrossRef]
26. Hassen, W.; Borjini, M.N.; Aissia, H.B. Enhanced heat transfer by unipolar injection of electric charges in differentially heated dielectric liquid layer. *FDMP Fluid Dyn. Mater. Process.* **2012**, *8*, 381–396.
27. Hassen, W.; Kolsi, L.; Oztop, H.F.; Al-Rashed, A.A.A.; Borjini, M.N.; Al-Salem, K. Electro-thermo-capillary-convection in a square layer of dielectric liquid subjected to a strong unipolar injection. *Appl. Math. Model.* **2018**, *63*, 349–361. [CrossRef]
28. Hassen, W.; Kolsi, L.; Ghachem, K.; Almeshaal, M.A.; Maatki, C.; Borjini, M.N. Numerical investigation of electro-thermo-convection in a square enclosure with incorporated hot solid body. *J. Therm. Anal. Calorim.* **2021**, *143*, 2647–2661. [CrossRef]
29. Borjini, M.N.; Abidi, A.; Aissia, H.B. Prediction of unsteady natural convection within a horizontal narrow annular space using the control-volume method. *Numer. Heat Transf. Part A* **2005**, *48*, 811–829. [CrossRef]
30. Patankar, S. *Numerical Heat Transfer and Fluid Flow*; Taylor & Francis: Oxford, UK, 2018.

31. Bejan, A. *Convection Heat Transfer*; John Wiley & Sons: Hoboken, NJ, USA, 2004.
32. Vázquez, P.A.; Georghiou, G.E.; Castellanos, A. Numerical analysis of the stability of the electrohydrodynamic (EHD) electroconvection between two plates. *J. Phys. D Appl. Phys.* **2008**, *41*, 175303. [CrossRef]
33. Hassen, W.; Borjini, M.N.; Traore, P.; Aissia, H.B. Electroconvection between coaxial cylinders of arbitrary ratio subjected to strong unipolar injection. *J. Electrostat.* **2013**, *71*, 882–891. [CrossRef]
34. Yaws, C.L. *Chemical Properties Handbook*; McGraw-Hill Education: New York, NY, USA, 1999.
35. Tobazeon, R. Electrohydrodynamic instabilities and electroconvection in the transient and AC regime of unipolar injection in insulating liquids: A review. *J. Electrostat.* **1984**, *15*, 359–384. [CrossRef]
36. Hassen, W.; Kolsi, L.; Mohammed, H.A.; Ghachem, K.; Sheikholeslami, M.; Almeshaal, M.A. Transient electrohydrodynamic convective flow and heat transfer of MWCNT-Dielectric nanofluid in a heated enclosure. *Phys. Lett. A* **2020**, *384*, 126736. [CrossRef]
37. Traoré, P.; Perez, A.; Koulova-Nenova, D.; Romat, H. Analyse par simulation numérique du développement de l'instabilité électro-convective d'une couche de liquide diélectrique infinie soumise à une injection unipolaire. *Comptes Rendus Mécanique* **2009**, *337*, 667–674. [CrossRef]
38. Wright, J.L. A correlation to quantify convective heat transfer between vertical window glazings. *ASHRAE Trans.* **1996**, *102*, 940–946.
39. Elsherbiny, S.M. Free convection in inclined air layers heated from above. *Int. J. Heat Mass Transf.* **1996**, *39*, 3925–3930. [CrossRef]
40. Khezzar, L.; Siginer, D.; Vinogradov, I. Natural convection of power law fluids in inclined cavities. *Int. J. Therm. Sci.* **2012**, *53*, 8–17. [CrossRef]